Hydration and Carbonation Reactions of Calcium Oxide by Weathering: Kinetics and Changes in the Nanostructure

V. Morales-Flórez[†,‡,*], A. Santos[§], I. Romero-Hermida[†,‡], L. Esquivias[†,‡]

† Departamento de Física de la Materia Condensada, Universidad de Sevilla, Av. Reina Mercedes, s/n, 41012, Seville, Spain

‡ Instituto de Ciencia de Materiales de Sevilla (CSIC/US), Av. Américo Vespucio, 49, 41092, Seville, Spain

§ Departamento de Ciencias de la Tierra, Universidad de Cádiz, Av. República Saharaui s/n, 11510 Puerto Real, Spain

ABSTRACT

The weathering reactions of hydration and carbonation of nanostructured calcium oxide with atmospheric moisture and carbon dioxide have been characterized. This work is the first-to-date combined kinetic and nanostructural research on CaO oriented to two key processes for different systems, i.e. hardening of construction materials and carbon mineral sequestration. The evolution of the precipitated crystalline phases was monitored by X-ray diffraction and thermogravimetry, along with structural characterization by nitrogen physisorption, electron microscopy and small-angle scattering. Complete hydration of the samples was always found prior to the onset of carbon sequestration, which depended on the nanostructure of the samples. Hence, carbonation started after 300 h of weathering for samples with a specific surface area of 40 m^2/g, whereas carbonation of the samples with 20 m^2/g occurred after 550 h. Full carbonation from atmospheric CO_2 (100% efficiency) was obtained in all cases. This combined research was completed by developing an empirical description of the weathering reactions in terms of a two-process Random Pore Model. Finally, this work aimed to determine the role of the nanostructure of samples based on industrial wastes as one of the most important factors for developing efficient carbon sequestration technologies.

* Corresponding Author. Tel: +34 954 550 946. Fax: +34 954 552 870. E-mail address: vmorales@us.es (V. Morales-Florez).

1. Introduction

The reactions of hydration and carbonation of calcium oxide are key steps for fundamental processes in very different systems, such as in construction materials or carbon capture and sequestration (CCS) technologies. The hardening, durability and the mechanical performance of structures based on hydrated lime mortars, cements or concrete are highly determined by these processes.[1,2] In addition, several CCS technologies[3-7] involving calcium oxide, such as flue gas separation by carbonation/calcinations loops or carbon mineral sequestration, are being deeply researched since the high concentration of CO_2 in the atmosphere is promoting climate change with a variety of hazardous consequences about society is continuously being warned.[8,9]

In particular, CO_2 mineral sequestration[10-13] deserves special attention as it is by far the most durable CSS technology and, indeed, a complementary technology to already implemented carbon storage plants. Although it has been proposed as a plausible procedure to mitigate increasing carbon emissions worldwide, currently, mineral sequestration by capturing CO_2 directly from the air[14-16] (with very low energy consumption) lacks the necessary technological efficiency which would allow it to be implemented on a large scale, mainly due to the costs and kinetics of the process. To solve these obstacles, alkaline-rich mineral wastes are being proposed as sequestration agents[6,17-19] in order to decrease the costs of an industrial scale-up. Moreover, the specific (reactive) surface area has been revealed as one of the key parameters that controls the rate and the efficiency of these reactions.[20-22] Therefore, the kinetic limitations may be overcome using nanostructured sequestration agents in order to deal with reaction rates at a human scale under atmospheric conditions (1 bar, 300 K and [CO_2] ~400 ppm). Finally, the possible added-value of sequestration by-products, mainly Ca and Mg carbonates, as raw materials for subsequent

processes, as construction[4,10] or paper industry,[23] will promote the deployment of this technology on an industrial scale.

This work focused on the kinetics of the weathering processes of nanostructured calcium oxide samples obtained from a calcium-rich by-product of the acetylene industry.[16] Acetylene produced via calcium carbide generates an aqueous suspension of calcium hydroxide that is very efficient for carbon sequestration by weathering, as it is able to capture up to 30% of the total CO_2 emissions of the synthesis process of the acetylene itself. The weathering of calcium oxide implies moisture adsorption and hydration, yielding calcium hydroxide, and carbonation, which involves CO_2 fixation, to produce calcium carbonate and release water. The net reaction can be represented by:

$$CaO + CO_2 + H_2O \leftrightarrow Ca(OH)_2 + CO_2 \leftrightarrow CaCO_3 + H_2O \qquad \text{[Eq. 1]}$$

Hydration and carbonation reactions may proceed by two different regimes: a first regime involving rapid chemical reaction and a second regime slowed down because of the formation of an impervious by-product layer.[5,24-26] This passivating layer can lead to pore closure, preventing the exposure of unreacted CaO to gases for further reaction, and therefore, the kinetics of the second regime became governed by the diffusion of ions through it. Nevertheless, it was found that this retardant phenomenon can be minimized in microstructured samples.[21,27] Moreover, the catalytic effect of water in the carbonation reaction is well known, [20,28,29] so the presence of liquid-like adsorbed water from atmospheric moisture allows Ca^{2+} and OH^- ions to be formed as a consequence of the solubility of the minerals and the subsequent precipitation of new minerals.

A simple method for researching the kinetics of the weathering reactions consists of accurately registering weight changes in samples exposed to atmospheric gases.[30,31] Based on these experiments, Aono proposed an exponential form for gas-solid kinetics under controlled atmospheres where the sample mass depends on time, $M \propto (1 - e^{-t/\tau})$. The characteristic kinetic

constant τ has been found to depend not only on the gas concentration, but also on the nanostructure of the sample.[20,24,32,33] In particular, for chemically identical samples, the difference between the reaction kinetics and efficiency can be explained in terms of differences in pore geometry or specific surface area.

But the nanostructure is a dynamic characteristic upon weathering.[28,34,35] To describe this phenomenon, different kinetic models have been proposed,[36,37] for example the Random Pore Model[38] (RPM), which has been considered in different systems, such as gas-solid carbonation kinetics of air pollution control residues[39] or carbonation-calcination cycles on calcium oxide.[5,40] The parameters of the RPM model are obtained as a function of the internal pore structure (porosity, pore distribution, specific surface area, etc.) of the pristine sample.

This work aimed to reveal the relationships between the kinetics and nanostructure of calcium oxide upon hydration and carbonation by weathering. Changes in the nanostructure (specific surface area, pore volume and particle size), morphology and crystalline phases were also analyzed. In addition, structural experimental data were considered for jointly modeling both reactions based on the RPM. Additionally, this work intended to provide valuable information in order to enhance the viability of CO_2 mineral sequestration technologies.

2. Materials and methods

2.1. Synthesis of highly reactive powders

The calcium-rich slurry (waste) from the acetylene industry was kindly supplied by AIR LIQUIDE España SA. X-ray fluorescence and X-ray diffraction analyses revealed a composition of portlandite (calcium hydroxide, $Ca(OH)_2$) above 95 wt.%. Reported structural analyses showed a high specific surface area (47.5 m^2/g) and the presence of submicrometric grains formed by bundles of sticks

smaller than 200 nm. This material was fully characterized and successfully tested as carbon sequestration agent by weathering.[16] The calcium-rich slurry was heat-treated in order to obtain nanostructured calcium oxide, CaO. Heat treatments involved t_h = 600 ^{o}C for 1 h (above the dehydroxylation temperature of portlandite[41]) or t_h = 800 ^{o}C for 1 h, to obtain samples with different nanostructures due to incipient sintering.[22,42] The samples will be referred as CaO600 and CaO800, respectively. A minimum of 15 samples was considered for each treatment to ensure reproducibility and for statistics. 300 ^{o}C, 500 ^{o}C and 1000 ^{o}C and 0 h, 0.5 h and 4 h were considered to check consistency, but no significant differences were observed regarding the subject of this work. All the obtained samples consisted of a fine white powder.

2.2. Weathering experiments

Immediately after heat treatment, two batches of the CaO were taken from the furnace and exposed to air, and one of them was placed on a precision balance. Special care was taken to equalize the fineness and compactness of the powder. The weathering reactions were researched by monitoring the weight of the first batch as a function of time for weathering intervals up to 4000 hours, whereas control samples were taken from the second batch to investigate changes in the structure or composition. Room conditions were kept constant at 25 ^{o}C and 50% relative humidity by an air conditioning system. Non-reactive porous silica was identically heat-treated and monitored in a balance to check the validity of the procedure.

2.3. Characterization methods

Samples were characterized by X-ray diffraction (XRD) with Cu K_α radiation, from 5.00^{o} to 70.00^{o} with a step size of 0.05^{o} and counting time of 80 s. In addition, the samples were characterized by nitrogen physisorption experiments, scanning electron microscopy (SEM) and small X-ray scattering (SAXS). Nitrogen physisorption experiments were performed at a constant temperature of 77.35 K.

Samples were degasified at 150 ^{o}C for two hours prior to the experiment. SEM was performed using an acceleration voltage of 2 kV. SAXS experiments were performed in the same device as the XRD analyses. The milled sample was enclosed with *Mylar* tape in the sample holder to protect the sample from weathering during the SAXS experiments. The SAXS device was previously tested and calibrated using a commercial colloidal silica sample of known particle size and shape.

Finally, the carbonation degree was estimated by thermogravimetric analyses (TGA) in a STD Q600 experimental device. The experiments were carried out under an N_2 flux of 100.0 ml/min, from ambient temperature up to 1000 ^{o}C, increased by 10 ^{o}C/min. To compare the experimental results with the theoretical maximum of the stoichiometric weight loss of a pure calcite sample due to decarbonation (44% between 550 ^{o}C and 900 ^{o}C), the mass of the samples was normalized to the weight of the dried sample at T = 200 ^{o}C.

2.4. Random Pore Model

The kinetic model reported by Bhatia and Perlmutter[38] was considered for describing the relationship between structure and kinetics. The simplified expression of the conversion degree upon a diffusion controlled regime as a function of time is:

$$\chi(t) = 1 - \Psi e^{-\omega(\sqrt{t}+\theta)^2} \qquad \text{[Eq. 2]}$$

Experimental data of the conversion degree $\chi(t)$ were obtained by direct comparison of the real-time mass variation data with the maximum mass variation (since this maximum corresponds to the mass of the completed reaction) in order to guarantee $\chi(t) \in [0,1]$. The relative error of conversion measurements was about $2 \cdot 10^{-3}$.

The 'structural parameter' Ψ, comprising the structural information regarding the specific surface area, porosity and the pore size distribution, was estimated from the experimental values

of the nanostructure obtained by nitrogen physisorption. The other two parameters, ω and θ, were obtained by numerical fitting. In the first approach, hydration and carbonation processes were considered to occur separately, so two different chemical processes were considered, but this point will be discussed later. Finally, a complete combined refining fitting was performed by the concatenation of both models.

3. Results and discussion

3.1. Real-time mass measurements

The sample mass was registered continuously, immediately after the heat treatment under room conditions and exposed to laboratory air. Representative curves of the two kinds of samples, CaO600 and CaO800, are plotted in Figure 1. The sample mass *M** was normalized to the initial mass, so mass changes can be easily compared with the stoichiometric values. Thus, a sample of pure calcium oxide (CaO) with a starting mass equal to 1 g will reach a mass of 1.32 g after complete hydration (total conversion into calcium hydroxide, $Ca(OH)_2$). Subsequent complete carbonation will increase the mass up to 1.79 g (complete conversion of 1 g of CaO into calcium carbonate, $CaCO_3$), neglecting the adsorbed moisture everywhere.

FIGURE 1

In all cases, the sample mass increased very fast during the first minutes, revealing extraordinary reactivity. In general, all the curves reproduced qualitative analogous behavior with the presence of two clearly separated steps. In addition, the values of the mass at the two plateaus were very close to the stoichiometric values of the fully reacted samples. These features suggest that weathering of CaO samples occurs in different phases: after initial moisture adsorption, fast hydration occurs (calcium hydroxide precipitation) taking up to several hundreds of hours, and once the hydration of

the sample is completed, carbonation takes place (calcium carbonate precipitation) over more than one month. The enormous differences between the water and carbon dioxide concentrations in the atmosphere generate the large difference between the characteristic times.

As a general consideration, a good correspondence between experimental and expected values of the mass can be concluded, but the M* values reached at the first plateau deserve special mention. They are slightly overestimated regarding the stoichiometric values due to moisture adsorption, being the overestimation slightly higher for CaO600 samples. This point can be understood in terms of the expected smaller structural features (less sintering) for samples treated at 600 ^{o}C with respect to 800 ^{o}C.[22,42] Regarding the final plateau, this difference was not present anymore, likely due to similar features in the final precipitated calcite. In addition, the formation of the calcium carbonate by-product enhanced the evaporation of adsorbed water,[28] reducing its relevance in the normalized mass. Finally, a mass of ~5 wt.% of impurities[16] was also present throughout the complete process, slightly shifting the normalized mass values.

Moreover, the lower heat treatment of the CaO600 samples led to faster kinetics of weathering with respect to the CaO800 samples, especially in terms of the slope at the initial stages (see inset of Fig. 1), and by reaching the plateaus sooner. This was also observed in the onset of carbonation. This feature can be numerically estimated by the change in the sign of the second time-derivative of M*. The estimated carbonation onsets were t = 300 ± 100 h and t = 550 ± 140 h for CaO600 and CaO800 samples, respectively. These differences confirm that reducing the heat treatment by 200 ^{o}C led to significant differences in the reactivity, as expected,[22,35,42] as samples calcined at lower temperature were more reactive due to their higher values of specific surface area.

The huge scientific production which refers to calcium hydroxide carbonation by atmospheric CO_2 deals with construction materials involving processes with takes several months or years. To

the best of our knowledge, this work is the first-to-date kinetic and nanostructure evolution joint research into calcium oxide oriented to the hydration and subsequent sequestration of atmospheric carbon dioxide. Although standard carbonation mineral sequestration experiments are usually performed at high CO_2 pressures or temperatures,[13,20,24,33,35,38,39,43] in our case, working under atmospheric conditions, the samples showed outstanding performance in terms of water adsorption and carbon sequestration.

3.2. Analysis of the samples

3.2.1. XRD analyses

The analyses revealed the evolution of different Ca-rich crystalline phases present in the sample during the weathering process. In Figure 2 left, diffraction patterns are shown for selected weathering times for a representative CaO800 sample (analogous results were obtained from CaO600 samples). In addition, semi-quantitative analyses of the XDR patterns gave an estimation of the relative concentration of the different observed phases. In Figure 2 right, the time dependences of the relative concentrations of CaO, $Ca(OH)_2$, and $CaCO_3$ for different sets of samples are plotted. It was confirmed that the samples were initially composed of CaO, remaining as the major phase up to weathering times below 2–3 h. The patterns obtained at later times revealed the gradual disappearance of CaO leading to $Ca(OH)_2$ precipitation (see Fig. 2 right for the quantitative time dependences). Then, $Ca(OH)_2$ remained as the most important phase up 100 h. This result confirms that the first plateau observed in the kinetic data of the normalized mass (Fig. 1) appears after complete hydration of the CaO sample, and prior to carbonation.

FIGURE 2

Regarding the onset of carbonation, XRD analyses revealed the presence of carbonate sooner in the CaO600 samples (Fig. 2 right), supporting the mass data analyses. In addition, the observation

of well-defined peaks of $CaCO_3$ after 720 h (Fig. 2, left) is also in good coherence with the carbonation onset estimated for CaO800 samples by the normalized mass curves (Fig. 1). Then, $Ca(OH)_2$ characteristic peaks disappeared progressively and $CaCO_3$ appeared as the unique final phase of the completed weathering process, beyond 500 h in the case of CaO600 samples, and beyond 900 h for the CaO800 ones. Detailed analyses revealed the presence of three calcium carbonate polymorphs (calcite, vaterite and aragonite; not shown). The different chemical conditions may yield to different polymorphs as well as hydrated amorphous carbonate phases,[2] but this point deserves a thorough crystallographic analysis. Finally, these results also indicate that full conversion of the calcium-rich phases into carbonate was achieved in all cases, suggesting the existence of a critical particle size below which the by-product layers do not impede the reactions to be completed and confirming these weathering processes as fully efficient carbon sequestration procedures.

3.2.2. Thermogravimetric analyses

The starting material (pure Ca-rich slurry, prior to any thermal treatment) presents, after drying, a unique weight loss of 22% at T = 400 ^{o}C due to the dehydroxylation of calcium hydroxide[41] (dashed line in Fig. 3). This value is very close to the dehydration stoichiometric mass loss of pure portlandite (24%), affected by the presence of some impurities.[16] After 312 h of weathering, the sample presented two weight losses of 5.6 wt.% at 400 ^{o}C and 30 wt.% at 750 ^{o}C, corresponding to the processes of dehydroxylation of $Ca(OH)_2$ and decarbonation of $CaCO_3$, respectively (red line in Fig. 3). The first weight loss indicates the presence of 23 wt.% of remaining hydroxide, and the second one confirms that the remaining 77 wt.% consisted of carbonate.

FIGURE 3

On the other hand, the presence of portlandite was negligible in the CaO600 sample weathered for 720 h (black line in Fig. 3), and only a weight loss of 40 wt.% was found a 750 ^{o}C, very close to the expected weight loss for a sample of pure $CaCO_3$ (44%), also affected by the presence of impurities. These results are in good coherence with the expected composition regarding the two-step weathering discussed regarding Figure 1, where CaO600 samples presented a mixed hydroxide/carbonate composition beyond 300 h and carbonation saturation beyond 600 h. In addition, these quantitative results confirmed the estimations by XRD (stars in Fig. 2, right).

3.3. Time-dependent structure

3.3.1. Nitrogen physisorption

As a general feature, it was confirmed that the increase in the characteristic size of the structural elements with heating temperature led to a decrease in the specific surface area and the pore volume, as expected. The time evolution of the specific surface area and the pore volume of different sets of CaO600 and CaO800 samples is plotted in Figure 4, left and in Figure A.1, respectively.

FIGURE 4

In view of these data, a general decreasing trend of these parameters was obviously concluded. Considering previous analysis which revealed the complete disappearance of CaO in order to form $Ca(OH)_2$ upon hydration and subsequently $CaCO_3$ upon carbonation, rather than structural evolution by a pore closure phenomena,[25,26] the original CaO grains turned into $Ca(OH)_2$ particles with a lower specific surface area and smaller pore volume. Afterwards, the formation of $CaCO_3$ continued in a similar fashion. Moreover, it is clear that the CaO600 samples had almost doubled values of the nanostructure parameters of the CaO800 samples, as expected.[22,42] Hence, the average specific surface area of the original samples was 37 ± 5 m^2/g and 20 ± 6 m^2/g, for the

CaO600 and CaO800 series, respectively. Both kinds of samples experienced a decrease of 40% in the specific surface area due to complete weathering. Regarding the pore volume, 0.32 ± 0.05 cm^3/g and 0.13 ± 0.04 cm^3/g were measured for the CaO600 and CaO800 sample series, respectively, with a decrease due to weathering of 50% in the case of the CaO600 samples and 33% in the CaO800 samples. Finally, it is worth noting that all these results are in good coherence with reported experiments on the nanostructure evolution of CaO.[33,42]

3.3.2. Small-angle X-ray scattering

Some selected curves of the SAXS intensity monitored for 100 h can be seen in Figure 4, right, involving complete hydration of the sample. There was a monotonous change in the scattering curves with time, and the well-defined Guinier region of the original sample (t = 0 h) gradually disappeared with time upon weathering,[44] suggesting the disappearance of well-defined CaO scatterers and the likely formation of larger structures. The estimated Guinier radii plotted in the inset of Figure 4, right confirm that during the first hours of weathering, the typical size of the nanostructure of the CaO remained constant at around $R_{Guinier}$ = 5.1 nm until hydration led to $Ca(OH)_2$ precipitation after t > 3 h of weathering, in agreement with the time-dependent data in Figure 2, right. At t = 100 h, CaO extinction was completed and $Ca(OH)_2$ formation occured with a characteristic size of $R_{Guinier}$ = 8.1 nm.

3.3.3. Scanning electron microscopy

In Figure 5 and Figure A.2, selected pictures of CaO800 samples are shown. At initial weathering (Fig. 5 top; Fig. A.2 top and middle), SEM revealed two existing morphologies: a gypsum flower-like phase, which has been associated with synthetic lime obtained from $Ca(OH)_2$ calcination,[45] and a particulate phase with a characteristic size of ca. 100 nm, associated with the $Ca(OH)_2$ observed by XRD (Fig. 2).

FIGURE 5

Further weathering up to 264 h led to $CaCO_3$ precipitation, coexisting with the remaining $Ca(OH)_2$. Spherulitic morphologies were identified as amorphous calcium carbonate,[2] as well as the rounded habits formed by vaterite arrangements[21,46] (Fig. 5, middle). Finally, at very long weathering times, typical calcite rhombohedra were the only observed morphologies (Fig. 5, bottom; Fig. A.2, bottom).

3.4. Two-step Random Pore Model

Two independent fittings based on the Random Pore Model[38] were performed for the hydration and carbonation reactions, separately. This assumption of separated processes is supported by all the previous experimental results, where two independent and consecutive reactions were identified. The hydration reaction was considered to be finished once the first plateau was reached, that is, at the time that the minimum value of the first derivative was reached. Then, the carbonation reaction was considered for the rest of the data. For both reactions, real-time mass data were normalized to the conversion reaction parameter $\chi(t)$, spanning from 0 to unity. This assumption of maximum conversion equaling unity is also supported by previous results which confirmed that the reactions were completed. In Figure 6, two representative experimental curves and their two-step model fittings are plotted. The very good correspondence between the mathematical model and the experimental values supports considering the diffusion regime of the Random Pore Model for these reactions.

FIGURE 6

The differences between characteristic reaction times ω^{-1} of the hydration and carbonation processes obtained upon fitting reflect the huge differences between H_2O and CO_2 concentrations in the atmosphere. The average hydration time was 40 h for both samples, despite the observed

structural differences between both kinds of samples. However, carbonation displayed clearly different kinetics: carbonation started sooner and was faster for the CaO600 samples, and the obtained carbonation characteristic times for the CaO600 and CaO800 samples were 200 h and 400 h, respectively. In Table A.1, all the fitting parameters are listed.

4. Conclusions

Mineralogical and structural characterizations of the hydration and the carbonation reactions of nanostructured CaO by weathering indicate that both processes take place separately and consecutively. Hence, the carbonation reaction does not start until the hydration of calcium oxide is completed. The small particle size and the nanostructure facilitate rapid reactions, full efficiency, and also prevent the passivating effect. The samples calcined at 600 ^{o}C presented an average specific surface area of 37 m^2/g, which corresponds to a carbonation onset at 300 h of weathering and full carbonation after 500 h, whereas samples calcined at 800 ^{o}C presented an average specific surface area of 20 m^2/g, which corresponds to a carbonation onset at 550 h of weathering and full carbonation after 900 h. The observed complete carbonation of these samples with a characteristic specific surface area typically above 20 m^2/g suggests the existence of a critical particle size above which the by-product layers will hinder the reactions, which could be estimated above ~90 nm. This feature also highlights the good performance of this sample as carbon sequestration agent by weathering, that is, under atmospheric conditions and without any energy supply required for the reaction to take place. These results have two technological implications: firstly, they highlight the importance of the structural features of industrial wastes to be considered as carbon sequestration agents; and secondly, they reveal full carbonation of this industrial waste by simple weathering as a sustainable source of calcite for subsequent industrial purposes.

Acknowledgements

The authors would like to thank AIR LIQUIDE España and the technical services of the ICMSE (CSIC/US) and CITIUS (US). VMF would like to thank the contract from V Plan Propio de Investigación of the Universidad de Sevilla (Spain). The funding from the project MAT2013-42934-R from the Spanish Ministry of Economy is also acknowledged.

Appendix A. Supplementary data

The evolution of the specific porous volume of the samples, measured by nitrogen physisorption, additional SEM images from CaO800 samples at 0.1 h and 4000 h of weathering, and the fitting parameters of the 2RPM. This material is available in the online version.

REFERENCES

1 H.F.M. Taylor, Cement Chemistry, Thomas Telford, London (UK), 1997.

2 O. Cizer, K. Van Balen, J. Elsen, D. Van Gemert, Real-time investigation of reaction rate and mineral phase modifications in lime carbonation, Constr. Build. Mater. 35 (2012) 741–751.

3 K.S. Lackner, A guide to CO_2 sequestration, Science 300 (2003) 1677–1678.

4 I.M. Power, A.L. Harrison, G.M. Dipple, S.A. Wilson, P.B. Kelemen, M. Hitch, G. Southam, Carbon mineralization: from natural analogues to engineered systems, Rev. Mineral. Geochem. 77 (2013) 305–360.

5 H. Gupta, L.S Fan, Carbonation-Calcination Cycle Using High Reactivity Calcium, oxide for Carbon Dioxide Separation from Flue Gas, Ind. Eng. Chem. Res. 41 (2002) 4035–4042.

6 W.J.J. Huijgen, G.J. Witkamp, R.N.J. Comans, Mineral CO_2 Sequestration by Steel Slag Carbonation, Environ. Sci. Technol. 39 (2005) 9676–9682.

7 P. Renforth, D.A.C. Manning, E. Lopez-Capel, Carbonate precipitation in artificial soils as a sink for atmospheric carbon dioxide, Appl. Geochem. 24 (2009) 1757–1764.

8 Intergovernmental Panel on Climate Change, Fifth Assessment Report of the IPCC, Cambridge University Press, New York (USA), 2013.

9 J. Hansen, and 17 more authors, Assessing ‘‘Dangerous Climate Change’’: Required Reduction of Carbon Emissions to Protect Young People, Future Generations and Nature, Plos ONE 8 (2013) e81648.

10 A. Olajire, A review of mineral carbonation technology in sequestration of CO_2, Energy Procedia 37 (2013) 6999–7005.

11 W. Seifritz, CO_2 disposal by means of silicates, Nature 345 (1990) 486.

12 K.S. Lackner, C.H. Wendt, D.P. Butt, E.L. Joyce, D.H. Sharp, Carbon dioxide disposal in carbonate minerals, Energy 20 (1995) 1153–1170.

13 V. Nikulshina, M.E. Gálvez, A. Steinfeld, Kinetic analysis of the carbonation reactions for the capture of CO_2 from air via $Ca(OH)_2$-$CaCO_3$-CaO solar thermochemical cycle, Chem. Eng. J. 129 (2007) 75–83.

14 J.K. Stolaroff, D.W. Keith, G.V. Lowry, Carbon dioxide capture from atmospheric air using sodium hydroxide spray, Environ. Sci. Technol. 42 (2008) 2728–2735.

15 R. Baciocchi, G. Storti, M. Mazzotti, Process design and energy requirements for the capture of carbon dioxide from air, Chem. Eng. Process. 45 (2006) 1047–1058.

16 V. Morales-Flórez, A. Santos, A. Lemus, L. Esquivias, Artificial weathering pools of calcium-rich industrial waste for CO_2 sequestration, Chem. Eng. J. 166 (2011) 132–137.

17 A. Kirchofer, A. Becker, A. Brandt, J. Wilcox, CO_2 mitigation potential of mineral carbonation with industrial alkalinity sources in the United States, Environ. Sci. Tecnol. 47 (2013) 7548–7554.

18 R. Pérez-López, G. Montes-Hernández, J.M. Nieto, F. Renard, L. Charlet, Carbonation of alkaline paper mill waste to reduce CO_2 greenhouse gas emissions into the atmosphere, Appl. Geochem. 23 (2008) 2292– 2300.

19 C. Cárdenas-Escudero, V. Morales-Flórez, R. Pérez-López, A. Santos, L. Esquivias, Procedure to use phosphogypsum industrial waste for mineral CO_2 sequestration, J. Hazard. Mater. 196 (2011) 431– 435.

20 K. Van Balen, Carbonation reaction of lime, kinetics at ambient temperature, Cem. Concr. Res. 35 (2005) 647–657.

21 A. Santos, M. Ajbary, V. Morales-Flórez, A. Kherbeche, M. Piñero, L. Esquivias, Larnite powders and larnite/silica aerogel composites as effective agents for CO_2 sequestration by carbonation, J. Hazard. Mater. 168 (2009) 1397–1403.

22 T.K. Bhattacharya, A. Ghosh, S.K. Das, Densification of reactive lime from limestone, Ceram. Int. 27 (2001) 455–459.

23 S. Teir, S. Eloneva, R. Zevenhoven, Production of precipitated calcium carbonate from calcium silicates and carbon dioxide, Energ. Convers. Manage. 46 (2005) 2954–2979.

24 S.M. Shih, C.S. Ho, Y.S. Song, J.P. Lin, Kinetics of the Reaction of $Ca(OH)_2$ with CO_2 at Low Temperature, Ind. Eng. Chem. Res. 38 (1999) 1316–1322.

25 J.M. Bukowski, R.L. Berger, Reactivity and strength development of CO_2 activated non-hydraulic calcium sililcates, Cem. Concr. Res. 9 (1979) 57–68.

26 H. Bearat, M. McKelvy, A. Chizmeshya, D. Gormley, R. Nunez, R.W. Carpenter, K. Squires, G.H. Wolf, Carbon Sequestration via Aqueous Olivine Mineral Carbonation: Role of Passivating Layer Formation, Environ. Sci. Technol. 40 (2006) 4802–4808.

27 V. Morales-Flórez, A. Santos, L. Esquivias, Recent insights into xerogel and aerogel mineral composites for CO_2 mineral sequestration, J. Sol-Gel Sci. Technol. 59 (2011) 417–423.

28 D.T. Beruto, R. Botter, Liquid-like H_2O adsorption layers to catalyze the $Ca(OH)_2/CO_2$ solid-gas reaction and to form a non-protective solid product layer at 20 ^{o}C, J. Eur. Ceram. Soc. 20 (2000) 497–503.

29 D. Daval, I. Martinez, J. Corvisier, N. Findling, B. Goffé, F. Guyot, Carbonation of Ca-bearing silicates, the case of wollastonite: Experimental investigations and kinetic modelling, Chem. Geol. 265 (2009) 63–78.

30 T. Aono, Studies on the reactions between gas and solid. Part I. Velocity of absorption of moisture by quicklime, B. Chem. Soc. Jpn. 6 (1931) 294–301; T. Aono, Studies on the reactions between gas and solid. Part II. Absorption of CO_2 by CaO and $Ca(OH)_2$, B. Chem. Soc. Jpn. 6 (1931) 319–324.

31 E. Rendek, G. Ducom, P. Germain, Carbon dioxide sequestration in municipal solid waste incinerator (MSWI) bottom ash, J. Hazard. Mater. B128 (2006) 73–79.

32 R.H. Borgwardt, R.D. Harvey, Properties of carbonate rocks related to SO_2 reactivity, Environ. Sci. Technol. 6 (1972) 350–360.

33 D. Beruto, M.G. Kim, A.W. Searcy, Microstructure and reactivity of porous and ultrafine CaO particles with CO_2, High Temp.– High Press. 20 (1988) 25–30.

34 V. Morales-Florez, N. Findling, F. Brunet, Changes on the nanostructure of cementitius calcium silicate, hydrates (C–S–H) induced by aqueous carbonation, J. Mater. Sci. 47 (2012) 764–771.

35 O. Regnault, V. Lagneau, H. Schneider, Experimental measurement of portlandite carbonation kinetics with supercritical CO_2, Chem. Geol. 265 (2009) 113–121.

36 S.K. Bhatia, J.S. Gupta, Mathematical-modelling of gas-solid reactions – Effect of pore structure, Rev. Chem. Eng. 8 (1992) 177–258.

37 D.K. Lee, An apparent kinetic model for the carbonation of calcium oxide by carbon dioxide, Chem. Eng. J. 100 (2004) 71–77.

38 S.K. Bathia, D.D. Perlmutter, Effect of the Product Layer on the kinetics of the CO_2-lime reaction, AiChe J. 29 (1983) 79–86.

39 V. Priggiobe, A. Polettini, R. Baciocchi, Gas-solid carbonation kinetics of air pollution control residues for CO_2 storage, Chem. Eng. J. 148 (2009) 270–278.

40 G. Grasa, R. Murillo, M. Alonso, J.C. Abanades, Application of the Random Pore Model to the carbonation cyclic reaction, AiChe J. 55 (2009) 1246–1255.

41 M. Arandigoyen, J.L. Pérez Bernal, M.A. Bello López, J.I. Alvarez, Lime-pastes with different kneading water: pore structure and capillary porosity, Appl. Surf. Sci. 252 (2005) 1449–1459.

42 J.M. Commandré, S. Salvador, N. Zihou, Reactivity of laboratory and industrial limes, Chem. Eng. Res. Des. 85 (2007) 473–480.

43 H. Lu, P.G. Smirniotis, F.O. Ernst, S.E. Pratsinis, Nanostructured Ca-based sorbents with high CO_2 uptake efficiency, Chem. Eng. Sci. 64 (2009) 1936–1943.

44 O. Glatter, O. Kratky, Small Angle X-ray Scattering, Academic Press, London (UK), 1982.

45 L. Bernard, M. Freche, J.L. Lacout, B. Biscans, Preparation of hydroxyapatite by neutralization at low temperature—influence of purity of the raw material, Powder Technol. 103 (1999) 19–25.

46 P. López-Arce, L.S. Gómez-Villalba, S. Martínez-Ramírez, M. Álvarez de Buergo, R. Fort, Influence of relative humidity on the carbonation of calcium hydroxide nanoparticles and the formation of calcium carbonate polymorphs, Powder Technol. 205 (2011) 263–269.

Graphical Abstract (for review)

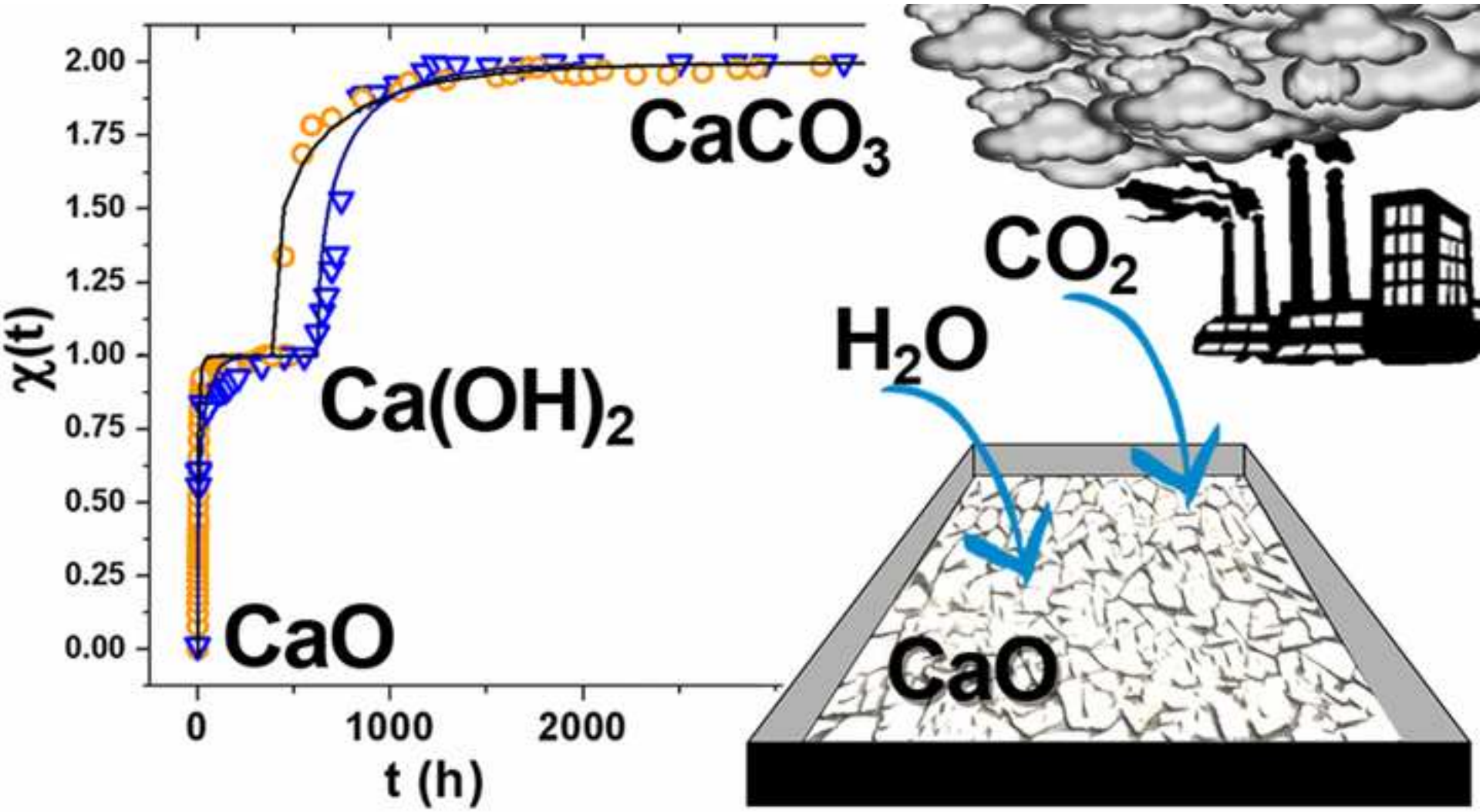

Figure captions

Figure 1. Normalized mass M* data for two representative samples of the sets CaO600 and CaO800. Masses were normalized to the starting values, so M*(t=0) = 1. Downward arrows mark the estimated time of carbonation onset. Inset magnifies first 200 h of weathering (dashed box).

Figure 2. Left: X-ray diffraction patterns of a CaO800 sample. Identified peaks correspond to the following patterns: L=Lime (CaO, PDF: 00-004-0777); P=Portlandite (Ca(OH)2, PDF: 01-089-2779 and 00-044-1481); C=Calcite (CaCO3, PDF: 01-086-0174). Right: time evolution of the relative presence of CaO, Ca(OH)2 and CaCO3. Open and solid symbols correspond for CaO600 and CaO800 samples, respectively. Curved lines are guides for the eye only.

Figure 3. Thermogravimetric analyses of the starting Ca-rich slurry (dried in an inert atmosphere) and of CaO600 sample weathered for 312 h and 720 h.

Figure 4. Left: specific surface area, where black squares correspond to CaO600 samples and red circles correspond to CaO800 samples. Lines are guides for the eye only. Results corresponding to a sample heat-treated at 500 oC for 1 h were plotted to show consistency. Right: Log-log time dependence of the SAXS patterns for a CaO800 sample. Inset: characteristic Guinier radii derived from the SAXS results.

Figure 5. SEM images from a CaO800 sample at different weathering times. Top: t = 0.25 h; middle: t = 264 h; bottom: t = 4000 h.

Figure 6. Conversion vs. time plots and two-step Random Pore Model (2RPM) fitting, for two representative samples heat treated at different temperatures. Carbonation conversion □(t) data were shifted +1, in order to obtain a realistic concatenated representation.

Figure 1

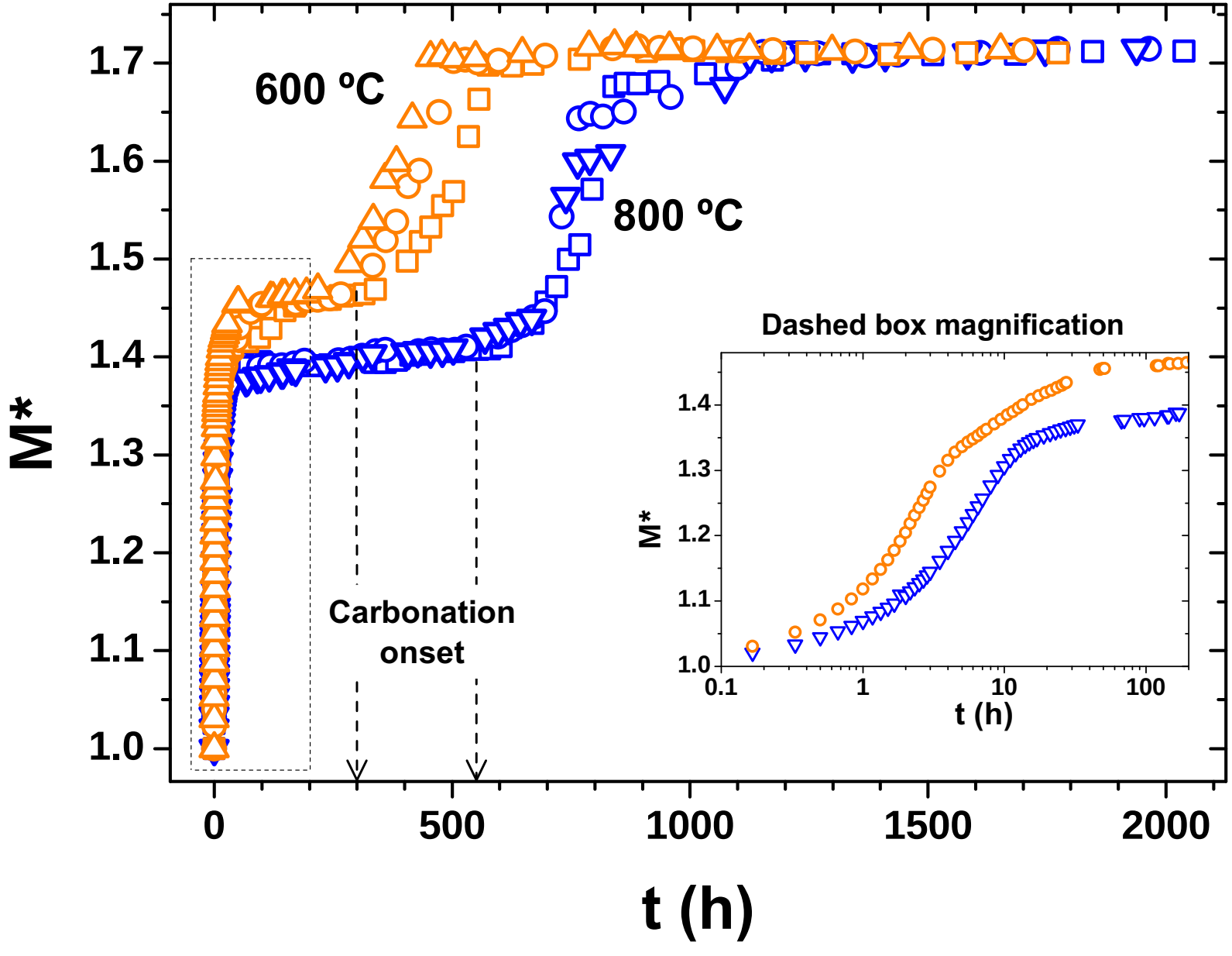
600 ºC
800 ºC
Carbonation onset
Dashed box magnification
M*
t (h)
1.0
1.1
1.2
1.3
1.4
1.5
1.6
1.7
0
500
1000
1500
2000
0.1
1
10
100

Figure 2

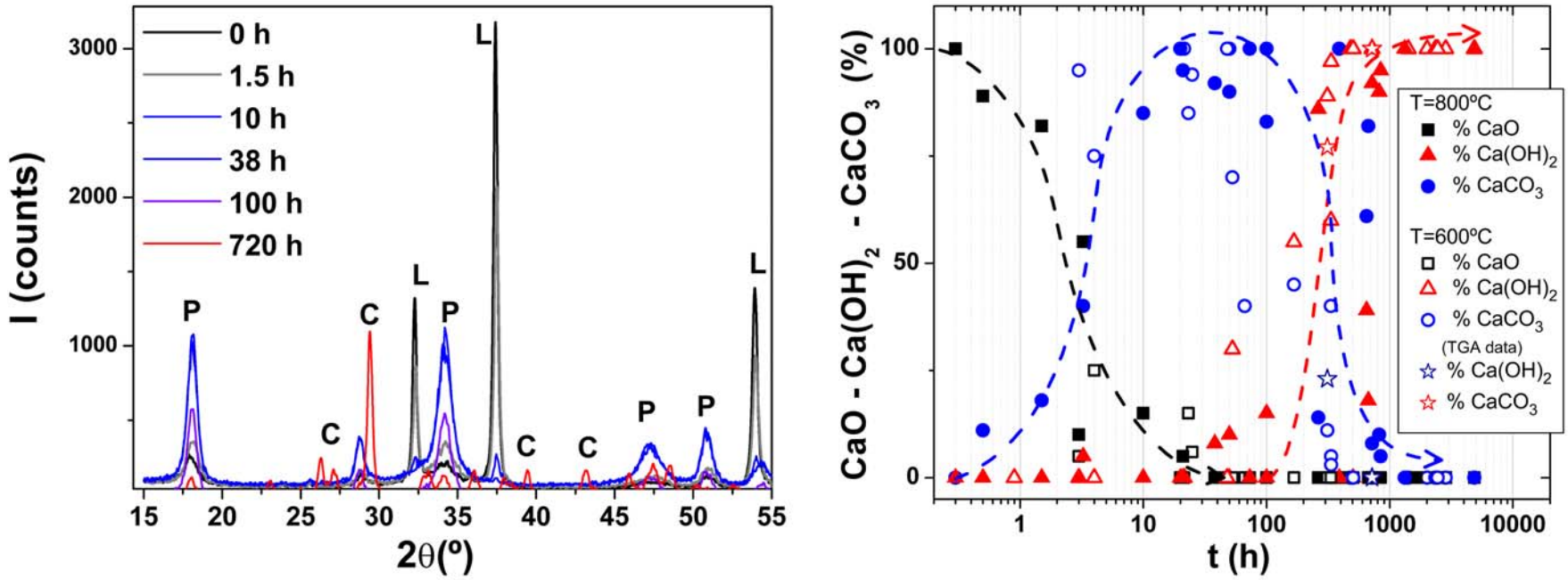
0 h
1.5 h
10 h
38 h
100 h
720 h
I (counts)
2θ(º)
P
C
L
T=800ºC
% CaO
% Ca(OH)2
% CaCO3
T=600ºC
% CaO
% Ca(OH)2
% CaCO3
(TGA data)
% Ca(OH)2
% CaCO3
CaO - Ca(OH)2 - CaCO3 (%)
t (h)

Figure 3

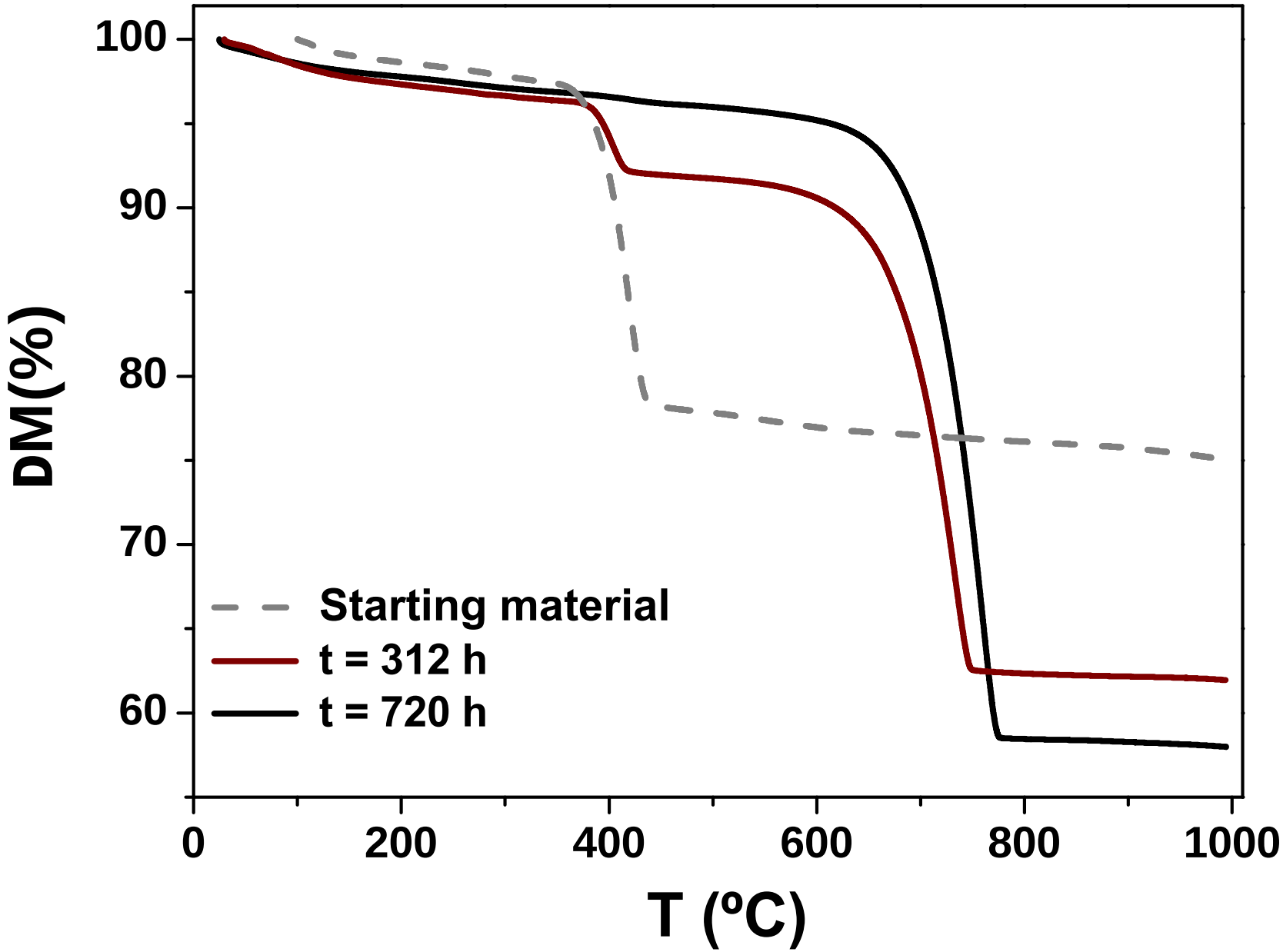
100
90
80
70
60
DM(%)
0
200
400
600
800
1000
T (ºC)
Starting material
t = 312 h
t = 720 h

Figure 4

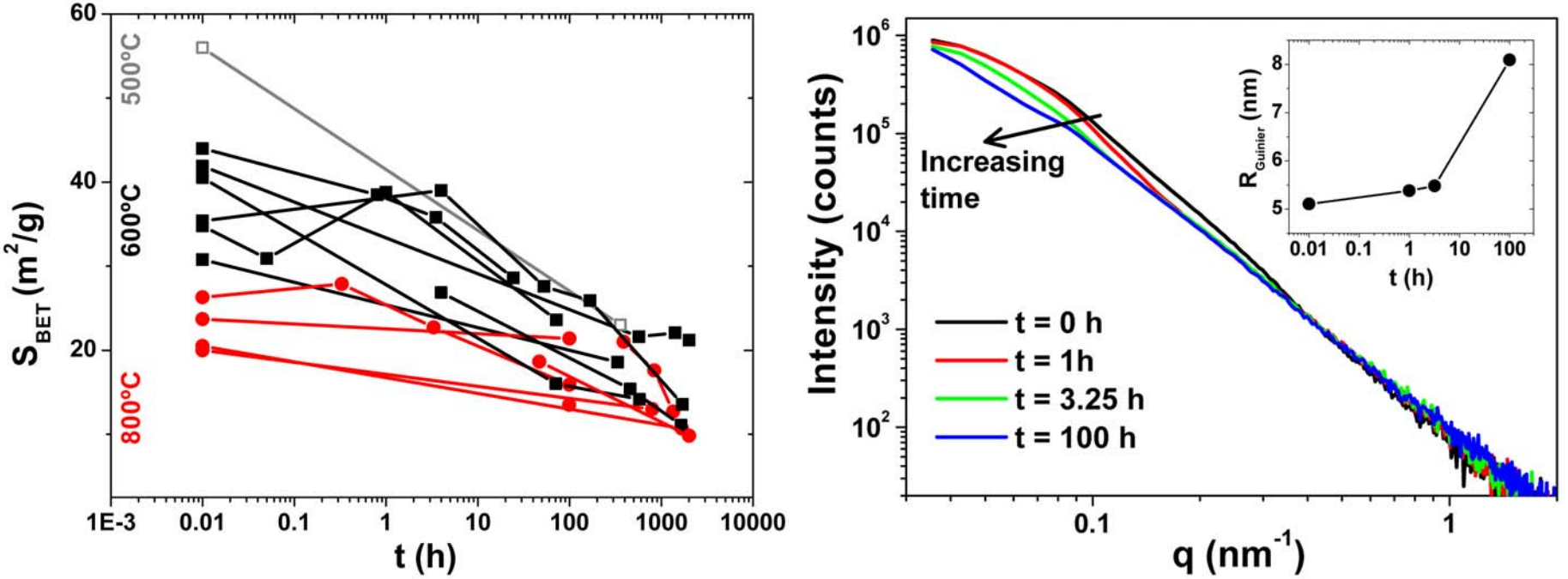
60
40
20
S_{BET} (m^2/g)
500°C
600°C
800°C
1E-3
0.01
0.1
1
10
100
1000
10000
t (h)
10^6
10^5
10^4
10^3
10^2
Intensity (counts)
Increasing time
t = 0 h
t = 1h
t = 3.25 h
t = 100 h
0.1
1
q (nm^{-1})
$R_{Guinier}$ (nm)
8
7
6
5
0.01
0.1
1
10
100
t (h)

Figure 5

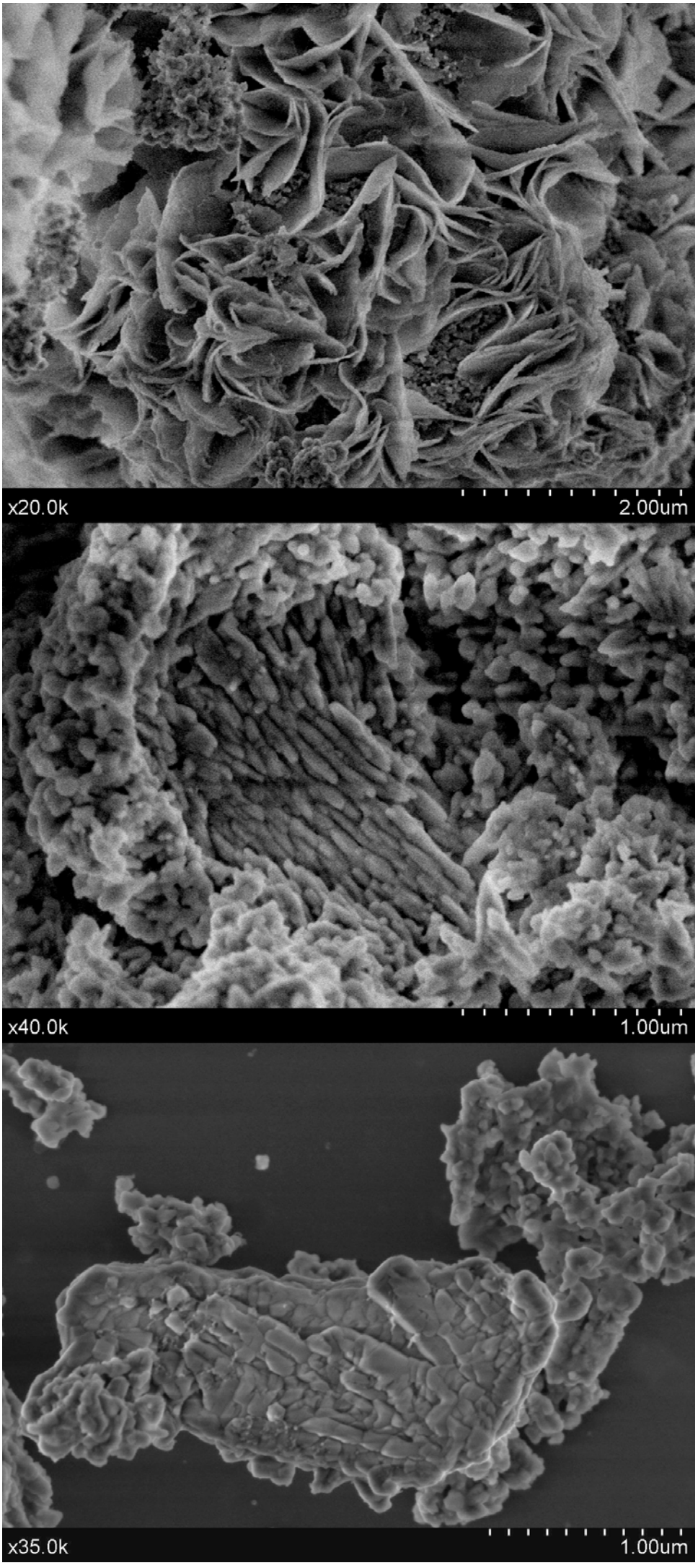

Figure 6

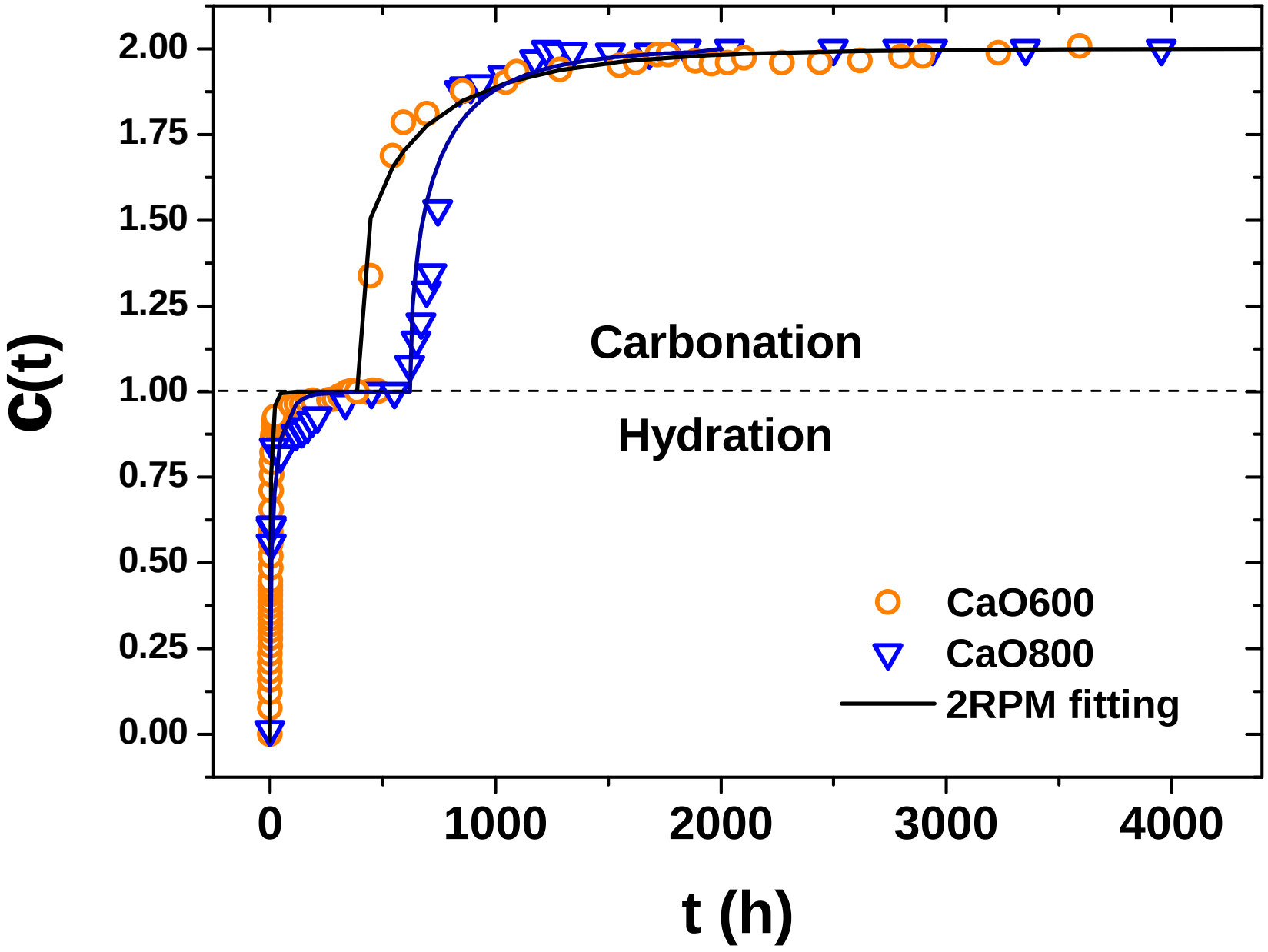
C(t)
2.00
1.75
1.50
1.25
1.00
0.75
0.50
0.25
0.00
Carbonation
Hydration
CaO600
CaO800
2RPM fitting
0
1000
2000
3000
4000
t (h)

Supplementary Material

Click here to download Supplementary Material: Nanostructure and kinetics of calcium oxide weathering_7.7_Supplementary.do